A&A 541, A73 (2012)
DOI: 10.1051/0004-6361/201118575

Astronomy & Astrophysics

Multi-line detection of O_2 toward ρ Ophiuchi A*

R. Liseau[1], P. F. Goldsmith[2], B. Larsson[3], L. Pagani[4], P. Bergman[5], J. Le Bourlot[6], T. A. Bell[7], A. O. Benz[8], E. A. Bergin[9], P. Bjerkeli[1], J. H. Black[1], S. Bruderer[8,21], P. Caselli[10], E. Caux[11], J.-H. Chen[2], M. de Luca[6], P. Encrenaz[4], E. Falgarone[12], M. Gerin[12], J. R. Goicoechea[7], Å. Hjalmarson[1], D. J. Hollenbach[13], K. Justtanont[1], M. J. Kaufman[14], F. Le Petit[6], D. Li[15,16], D. C. Lis[16], G. J. Melnick[17], Z. Nagy[18], A. O. H. Olofsson[5], G. Olofsson[3], E. Roueff[6], Aa. Sandqvist[3], R. L. Snell[19], F. F. S. van der Tak[18], E. F. van Dishoeck[20,21], C. Vastel[11], S. Viti[22], and U. A. Yıldız[20]

(Affiliations can be found after the references)

Received 4 December 2011 / Accepted 7 March 2012

ABSTRACT

Context. Models of pure gas-phase chemistry in well-shielded regions of molecular clouds predict relatively high levels of molecular oxygen, O_2, and water, H_2O. These high abundances imply high cooling rates, leading to relatively short timescales for the evolution of gravitationally unstable dense cores, forming stars and planets. Contrary to expectations, the dedicated space missions SWAS and Odin typically found only very small amounts of water vapour and essentially no O_2 in the dense star-forming interstellar medium.
Aims. Only toward ρ Oph A did Odin detect a very weak line of O_2 at 119 GHz in a beam of size 10 arcmin. The line emission of related molecules changes on angular scales of the order of some tens of arcseconds, requiring a larger telescope aperture such as that of the *Herschel* Space Observatory to resolve the O_2 emission and pinpoint its origin.
Methods. We use the Heterodyne Instrument for the Far Infrared (HIFI) aboard *Herschel* to obtain high resolution O_2 spectra toward selected positions in the ρ Oph A core. These data are analysed using standard techniques for O_2 excitation and compared to recent PDR-like chemical cloud models.
Results. The $N_J = 3_3 - 1_2$ line at 487.2 GHz is clearly detected toward all three observed positions in the ρ Oph A core. In addition, an oversampled map of the $5_4 - 3_4$ transition at 773.8 GHz reveals the detection of the line in only half of the observed area. On the basis of their ratios, the temperature of the O_2 emitting gas appears to vary quite substantially, with warm gas ($\gtrsim$50 K) being adjacent to a much colder region, of temperatures lower than 30 K.
Conclusions. The exploited models predict that the O_2 column densities are sensitive to the prevailing dust temperatures, but rather insensitive to the temperatures of the gas. In agreement with these models, the observationally determined O_2 column densities do not seem to depend strongly on the derived gas temperatures, but fall into the range $N(O_2) = 3$ to $\gtrsim 6 \times 10^{15}$ cm^{-2}. Beam-averaged O_2 abundances are about 5×10^{-8} relative to H_2. Combining the HIFI data with earlier Odin observations yields a source size at 119 GHz in the range of 4 to 5 arcmin, encompassing the entire ρ Oph A core. We speculate that one of the reasons for the generally very low detection rate of O_2 is the short period of time during which O_2 molecules are reasonably abundant in molecular clouds.

Key words. ISM: abundances – ISM: molecules – ISM: lines and bands – ISM: clouds – ISM: individual objects: ρ Oph A SM 1 – stars: formation

1. Introduction

Despite the universal importance of oxygen, its molecular form, O_2, is an elusive species of the interstellar medium (ISM). This molecule was thought to be one of the main regulators of the energy balance in the ISM, as summarised by Goldsmith & Langer (1978). Consequently, large efforts, from both the ground ($O^{18}O$) and space, were made to obtain quantitative estimates of its abundance. The historical account of this essentially fruitless "O_2-struggle" was reviewed by Goldsmith et al. (2011). Prior to *Herschel*, both SWAS (Melnick et al. 2000; Goldsmith et al. 2000) and Odin (Nordh et al. 2003; Pagani et al. 2003) had already shown that the abundances of both O_2 and H_2O assumed by Goldsmith & Langer (1978) were much higher than actual values in the ISM and, with the exception of the ρ Oph cloud, none of the O_2 lines were detected anywhere in the ISM. Goldsmith et al. (2002) announced the tentative detection by SWAS of the O_2 487 GHz line in ρ Oph A. The claimed signal appeared at an unusual velocity and was atypically broad. Pagani et al. (2003) showed that, based on more sensitive O_2 119 GHz observations with Odin, this was an erroneous result. This line was finally detected by Odin, at the correct local standard of rest (LSR) velocity and with a plausible, narrow line-width (Larsson et al. 2007). Here we report the detection of two more O_2 transitions in ρ Oph A, viz. at 487 GHz and at 774 GHz, respectively.

Besides being relatively nearby (120–130 pc, Lombardi et al. 2008; Snow et al. 2008; Mamajek 2008; Loinard et al. 2008), the ρ Oph cloud distinguishes itself from other low-mass star-forming regions in that it exhibits evidence (e.g., in $C^{18}O$ line emission) of gas at relatively high temperatures ($T \geq 20$ K) over extended regions with high column densities ($N(H_2) \gg 10^{22}$ cm^{-2}, Liseau et al. 2010). In addition, ρ Oph A displays an interesting chemistry: doubly deuterated formaldehyde (D_2CO) and hydrogen peroxide (H_2O_2) molecules, rarely seen elsewhere in the ISM,

* Based on observations with *Herschel*-HIFI. *Herschel* is an ESA space observatory with science instruments provided by European-led Principal Investigator consortia and with important participation from NASA.

Table 1. Instrumental reference.

Transition[a] $N_J^{\rm up} - N_J^{\rm low}$	Frequency[b] ν_0 (MHz)	Wavelength λ_0 (μm)	Energy $E_{\rm up}/k$ (K)	Observatory/ Instrument	Beam width HPBW (′)	Efficiency $\eta_{\rm mb}$	Reference
1_1-1_0	118750.341	2526	5.7	Odin	9.96	0.91	Frisk et al. (2003)
3_3-1_2	487249.264	616	26.4	SWAS	3.5×5.0	0.90	Melnick et al. (2000)
				HIFI	0.73	0.757	Roelfsema et al. (2012)
5_4-3_4	773839.512	388	60.7	HIFI	0.47	0.753	Roelfsema et al. (2012)

Notes. [a] An energy level diagram is provided by, e.g., Goldsmith et al. (2011). [b] Frequencies are from the JPL-catalogue http://spec.jpl.nasa.gov/cgi-bin/catform

Table 2. Source designations and coordinates for ρ Oph A, with positions observed in O_2 in bold face.

RA (h m s) J2000.0	Dec (° ′ ″) J2000.0	Source designation	Reference
16 25 24.32	–24 27 56.57	HD 147889	SIMBAD: http://simbad.u-strasbg.fr/simbad/
16 26 17.5	–24 23 13	H 4, HH 313B	Dent et al. (1995), Caratti o Garatti et al. (2006)
16 26 19.0	–24 23 08	H 5, HH 313A	Dent et al. (1995), Caratti o Garatti et al. (2006)
16 26 21.36	–24 23 06.4	GSS 30, El 21	Grasdalen et al. (1973), Elias (1978)
16 26 25.7	**–24 23 24**	**O1**	this paper
16 26 25.7	**–24 23 57**	**O2**	this paper
16 26 26.1	–24 23 14	N_2H^+ N1 b (*FWHM* = 0.29 km s^{-1})	di Francesco et al. (2004)
16 26 26.38	–24 24 31.0	VLA 1623	André et al. (1990)
16 26 27.1	–24 23 30	N5, 850 μm	di Francesco et al. (2004), Johnstone et al. (2000)
16 26 27.2	–24 24 04	Deuterium peak	Bergman et al. (2011a)
16 26 27.3	–24 23 28	SM 1N, 1.3 mm	Motte et al. (1998)
16 26 27.9	**–24 23 26**	**O3**, P2, $C^{18}O$ (3 - 2)	this paper, Liseau et al. (2010)
16 26 27.9	**–24 23 57**	**O4**, P3, $C^{18}O$ (3 - 2); SM 1, 1.3 mm	this paper, Liseau et al. (2010), Motte et al. (1998)
16 26 34.19	–24 23 28.2	S 1, GSS 35, El 25	Grasdalen et al. (1973), Elias (1978)

have for example been found here (Bergman et al. 2011a,b). The overall impression is that the observable abundance of many species is the result of surface reactions on dust grains, a process that may also pertain to the production of oxygen molecules.

The first motivation behind our *Herschel* observations was to pin down the precise location of the O_2 source inside the large, ten-arcminute beam of Odin. Secondly, we wished to add observations of the O_2 487.25 GHz (3_3-1_2) and 773.84 GHz (5_4-3_4) lines, which have upper level energies $E_{\rm up}/k$ = 26 K and 61 K, respectively, to the Odin data of the 118.75 GHz (1_1-1_0) transition ($E_{\rm up}/k$ = 6 K). These observations should enable us to learn something about the nature of the O_2 source in the ρ Oph cloud. This could then be compared to the physical and chemical conditions of other locations in the general ISM and potentially identify the characteristics and timescales of regions containing O_2 molecules.

The paper is organised as follows: in Sect. 2, our *Herschel*-HIFI observations and their reduction are discussed in considerable detail and our results are presented in Sect. 3. These results are discussed in Sect. 4, where the spectral line formation is analysed under different assumptions. Finally, in Sect. 5, our main conclusions are briefly summarised.

2. Observations and data reduction

Herschel is a space platform for far-infrared and sub-millimetre observations (Pilbratt et al. 2010). It orbits the Sun about 1.5 million kilometres beyond the Earth (at L 2) and its 3.5 m primary dish is radiatively cooled to its operational equilibrium temperature of about 85 K. The scientific instruments are placed in a liquid-helium-filled cryostat, limiting its cold lifetime to roughly 3.5 years. One of the three onboard instruments is the Heterodyne Instrument for the Far Infrared (HIFI, De Graauw et al. 2010) with continuous frequency coverage from 480 GHz to 1250 GHz ($\lambda\lambda$ 624–234 μm) in 5 bands. In addition, the frequency range 1410 GHz to 1910 GHz ($\lambda\lambda$ 213–157 μm) is covered by bands 6 and 7. The spectral resolving capability is the highest available on *Herschel*, i.e. up to 10^7 corresponding to 30 m s^{-1}, and is required to resolve the profiles of very narrow lines of cold sources, which have temperatures of the order of 10 K or less.

Spectral line data and the relevant characteristics of the instruments discussed in this paper have been compiled in Table 1.

2.1. The 487 GHz observations

The 487 GHz observations with HIFI were performed on operating day OD 673 (2011 March 18). The three positions O1, O3, and O4 at the centre of the ρ Oph A core (Table 2) were observed in double beam-switch mode (DBS), with beam throws of 3′ in roughly the west and east directions (with a position angle of 101° E of N) and identified in Fig. 1 by the numbers 6031 and 6032, respectively. For each position, the relative observing time spent on the east- and westward on-off pairs was 7.3 h, and the total programme execution time was 21.9 h. The DBS mode generally produces the highest quality data with HIFI and since the O_2 signal is known to be weak, this was the observing mode chosen. Switching by only three arcminutes inside a molecular cloud is generally considered not to be a sensible option, as this potentially results in the cancellation of the source signal. However, a relatively large velocity gradient ($\gtrsim$0.3 km s^{-1}/arcmin) and/or two distinctly different velocity systems ($\Delta\upsilon \sim$ 1 km s^{-1}) are known to exist in ρ Oph A (e.g., Bergman et al. 2011a). In addition, the O_2 line is known to be narrow (*FWHM* $\sim$ 1 km s^{-1}). Hence, all of these factors taken together suggest that the risk of signal cancellation is low. Splitting the entire data set into two and reducing these two halves with only one of the off-spectrua used resulted in essentially the

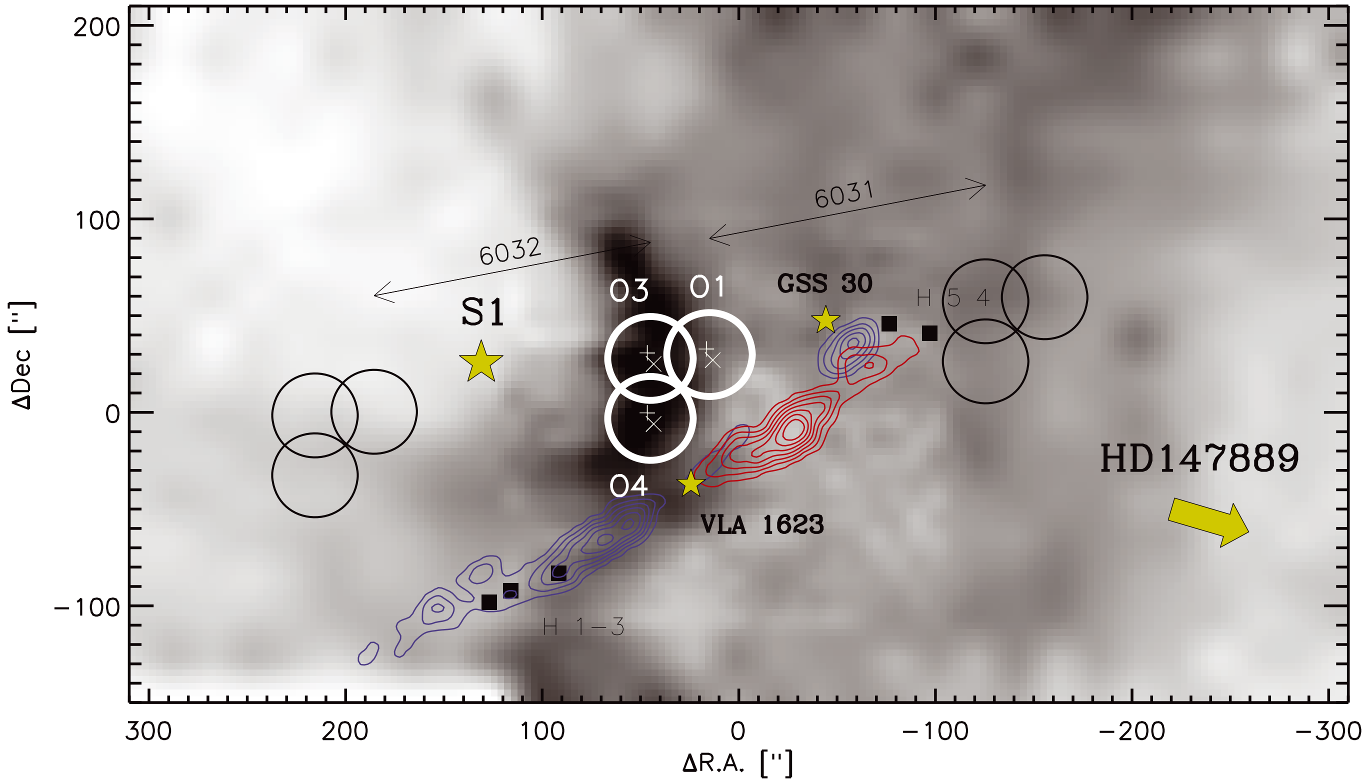

Fig. 1. *Herschel* beams of O_2 487 GHz (44″) superposed onto a grey scale $C^{18}O$ (3−2) map of ρ Oph A (Liseau et al. 2010). The + and × symbols designate the positions of the H- and V-polarization beam centres of HIFI, respectively, with a separation of 6.″6. The heavy circles show the positions of the sources O1, O3, and O4 (see Table 2), with the corresponding off-source reference positions shown by the displaced symbols to the east and west and identified by their observation numbers, 6032 and 6031 respectively, above the double arrows. The origin is at $16^h26^m24^s.6$, −24°23′54″ J(2000.0) and offsets in RA and Dec are in arcsec. At the distance of 120 pc, 40″ corresponds to about 0.02 pc. The star symbols identify the positions of the star S 1, the young stellar object GSS 30 and the Class 0 source VLA 1623, where the contours depict red- and blueshifted CO (3−2) emission of its bipolar outflow. The filled squares identify the known Herbig-Haro objects H1 through 5 and the direction to the dominating B-star HD 147889, about 15′ away, is indicated by the heavy arrow.

same spectral data. These off-beams were pointed at very different regions in ρ Oph A (Fig. 1), but no traceable off-beam contamination was introduced by the DBS observations.

The receivers are double side-band and to counteract confusion in frequency space, we selected for each observation 8 different LO-tunings inside HIFI-band 1a, spaced by 170 MHz to 260 MHz. During data reduction, this allowed us to perform a sideband deconvolution and identify any "false" signal due to a strong feature in the other sideband, which might otherwise have been folded over onto the weak O_2 feature.

We used both the Wide Band Spectrometer (WBS) and the High Resolution Spectrometer (HRS) with respective resolutions 1.10 MHz and 250 kHz (0.68 and 0.15 km s^{-1}). The positions of spikes and spectrometer artifacts are known and flagged, and none of these interfered with the O_2 observations. Initial data reduction and calibrations were performed with the standard *Herschel* pipeline HIPE version 7.1 and the subsequent data analysis was made with a variety of other software packages. The quality of the HIFI data is excellent and it was sufficient to subtract a low-order baseline for each LO setting prior to averaging. The intensity calibration accuracy is estimated to be 10%.

The frequency-dependent beam widths (HPBW) and main beam efficiencies (η_{mb}) were adopted from Roelfsema et al. (2012). Before averaging the data for a given position, the H- and V-polarization spectra were all inspected individually in order to avoid the suppression of weak spectral lines or the generation of artificial features.

2.2. 774 GHz observations

The 774 GHz observations with HIFI band 2 were made on OD 583 (2011 September 15). A 6 × 6 map, aligned with the equatorial celestial coordinates (Fig. 3), was obtained with a 10″ regular spacing, oversampling the 28″ beam by nearly a factor of three and allowing for potentially increased spatial information of the emission regions.

Both the WBS (0.43 km s^{-1}) and the HRS (0.097 km s^{-1}) were used. The 774 GHz data were also obtained in DBS mode, with the offset positions displaced by 3′ and in nearly the same chopping direction as before (along PA = 98°). With 500 s on-source integrations at each position, the total observing time was 12 h.

3. Results

In the figures showing HIFI data, brightness is given as the antenna temperture, T_A. When more than one telescope had been used, the data are presented on the main beam brightness temperature scale, T_{mb}, where the main-beam efficiency is η_{mb} = 0.75 for both HIFI transitions (Roelfsema et al. 2012) and 0.9 for the Odin transition (Frisk et al. 2003; Hjalmarson et al. 2003) and where we use the relation $T_A/\eta_{mb} = T_{mb}$. For completeness, we also provide in Table 3, together with the HIFI data, the results of the Odin observations.

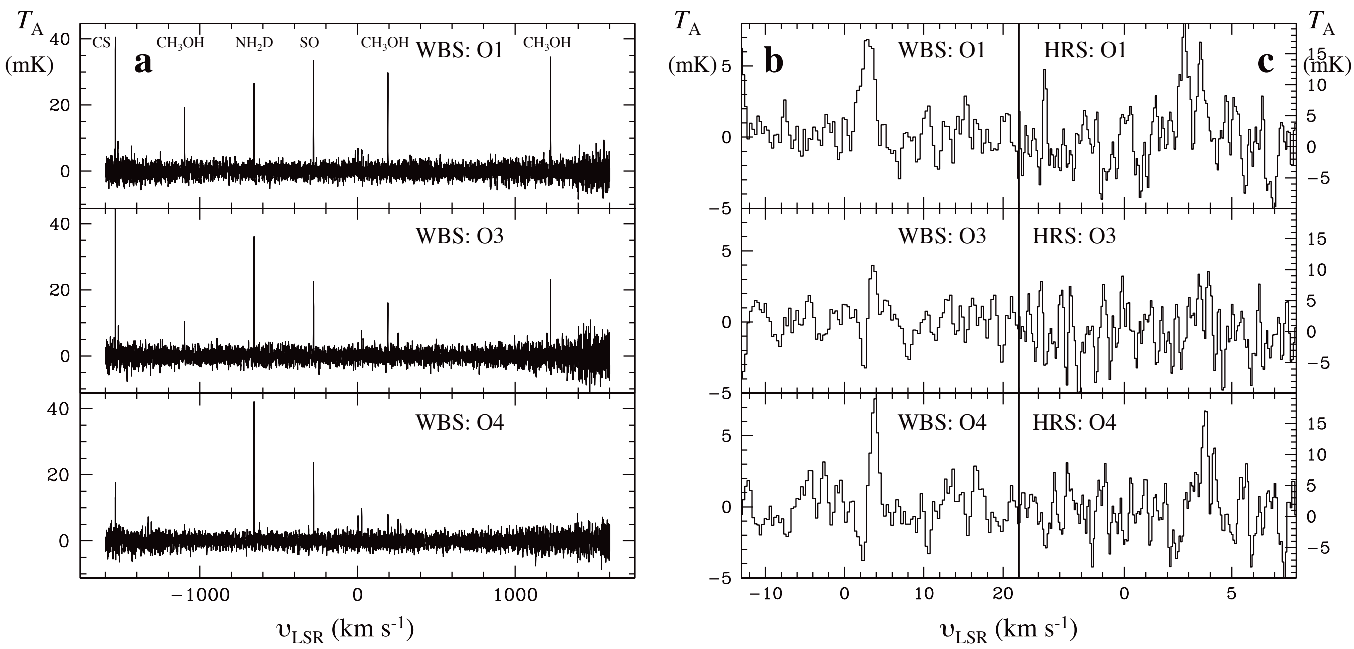

Fig. 2. Average double side band (DSB) spectra of H- and V-polarizations for the three positions O1, O3, and O4 in the ρ Oph A cloud core, shown for the range 484.65 GHz to 489.85 GHz. The spectral lines are found exclusively in the lower side band (LSB) and the LSR velocity, $\upsilon_{\rm LSR}$, along the abcissa is in km s^{-1} and the antenna temperature $T_{\rm A}$ along the ordinate in mK. **a)** 5 GHz wide band of the WBS around the 487 O_2 line (-1600, $+1600$ km s^{-1}). **b)** The WBS spectrum at expanded scale, showing the O_2 line at 487 GHz, which is detected in all three positions. Inspection of the individual on-off pairs suggests that the apparent absorption features next to the lines are not real but simply due to the noise. **c)** Similar to **b)** but for the corresponding HRS data.

Table 3. O_2 line observations of ρ Oph A.

Position/ Average	$T_{\rm mb,0}$[a] (mK)	$\upsilon_{\rm LSR}$[a] (km s^{-1})	*FWHM*[a] (km s^{-1})	$10^3 \int T_{\rm mb}\,d\upsilon$ (K km s^{-1})
	487 GHz	$N_J = 3_3 - 1_2$		
O1 HRS	14.4 ± 1.8	3.05 ± 0.10	1.63 ± 0.23	19.8 ± 2.4
O1_1[b]	24.2 ± 3.3	2.79 ± 0.05	0.46 ± 0.08	15.5 ± 1.7
O1_2	19.6 ± 3.5	3.58 ± 0.04	0.41 ± 0.09	8.7 ± 1.7
O3 HRS	7.6 ± 2.2	3.59 ± 0.12	0.80 ± 0.27	5.7 ± 1.3
O4 HRS	11.5 ± 2.5	3.75 ± 0.07	0.84 ± 0.16	13.0 ± 1.6
O1 WBS	9.4 ± 2.0	2.89 ± 0.20	1.91 ± 0.46	18.4 ± 1.6
O1_1	9.6 ± 1.4	2.70 fix	0.90 fix	9.2 ± 1.4
O1_2	6.9 ± 1.4	3.60 fix	0.90 fix	6.6 ± 1.4
O3 WBS	5.7 ± 3.4	3.66 ± 0.26	0.87 ± 0.60	5.3 ± 1.5
O4 WBS	10.3 ± 2.6	3.78 ± 0.12	0.99 ± 0.28	10.3 ± 1.5
⟨O3, O4⟩WBS	7.8 ± 3.0	3.69 ± 0.20	0.90 ± 0.47	7.8 ± 1.5
	774 GHz	$N_J = 5_4 - 3_4$		
⟨O1, O2⟩HRS	22.3 ± 9.9	3.59 ± 0.03	0.57 ± 0.10	13.2 ± 4.0
O1 WBS	17.9 ± 4.2	3.66 ± 0.07	0.61 ± 0.16	11.4 ± 2.9
O2 WBS	14.5 ± 3.8	3.59 ± 0.09	0.72 ± 0.22	10.9 ± 2.8
⟨O1, O2⟩WBS	15.9 ± 2.8	3.62 ± 0.06	0.67 ± 0.17	11.2 ± 2.0
O3 WBS	…	…	…	3.6 ± 2.9
O4 WBS	…	…	…	-1.6 ± 3.0
⟨O3, O4⟩WBS	…	…	…	0.8 ± 2.0
	119 GHz	$N_J = 1_1 - 1_0$		
Odin[c]	19.3 ± 0.6	3.5 ± 0.5	1.5 ± 0.5	26.7 ± 4.4

Notes. [(a)] Gaussian fits: peak intensity, central velocity and full width half maximum of line. [(b)] O1_1 and O1_2 refer to two velocity components (see Sect. 3.1). [(c)] 10′ beam centred on ρ Oph A (Larsson et al. 2007).

3.1. 487 GHz

The reduced WBS spectra for the three positions O1, O3, and O4 are shown for the frequency range 484.65 GHz to 489.85 GHz in Fig. 2a. The upper side band (USB) is completely line-free, i.e. all line detections refer to the LSB only. The presented data are DSB in order to suppress the noise. Centred on the O_2 line, radial velocities span -1600 to $+1600$ km s^{-1}. In addition to the detected O_2 487.25 GHz lines near an LSR velocity of 3 km s^{-1} in all three positions, the spectra show a number of other emission features that correspond to identified molecular lines, of, e.g., CS, CH_3OH, NH_2D, and SO, to mention only the strongest ones. In addition these spectra reveal variations in intensity and line width on angular scales of only some tens of arcsec. The remarkable behaviour of these different molecular species toward the ρ Oph A core has been known for some time, and was recently documented by Bergman et al. (2011a). Our multi-line HIFI data will not be discussed further here but will be presented elsewhere (Larsson et al.; Pagani et al., in prep.).

Figure 2b shows the WBS spectra zoomed in on the O_2 487 GHz transition. The intensity of this line also varies at the three positions. In particular, the line toward the O1 position appears, by comparison, rather strong and broader than those toward O3 and O4. The HRS data shown in Fig. 2c suggest that the line at O1 is a composite of two different, narrow components, blended into a single broad feature at the lower resolution of the WBS. Henceforth, we refer to this spectral component at $\upsilon_{\rm LSR} \sim +3.6$ km s^{-1} as O1_2, whereas the one closer to 2.8 km s^{-1} is referred to as O1_1.

We summarise the spectral characteristics of the O_2 487 GHz line in Table 3. Within the errors, the WBS line centroids and widths agree with the Gaussian fittings of the HRS data. In addition, the average intensities at the positions O1_2, O3, and O4 with the WBS (8.3 ± 1.8 mK km s^{-1}) and the HRS (9.1 ± 1.9 mK km s^{-1}), respectively, are consistent with each other.

In addition, the O_2 line centroid and width also conform with values of other optically thin species, e.g. $^{13}C^{18}O$ (3–2)

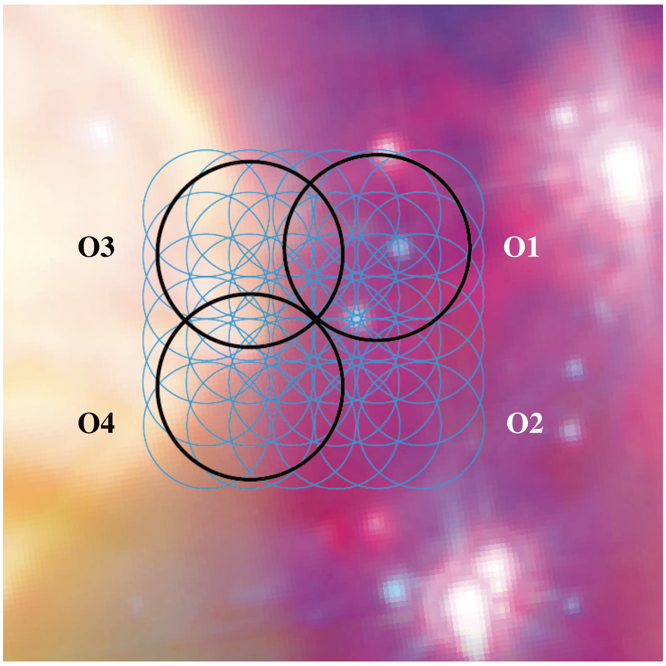

Fig. 3. Outline of the oversampled 6 × 6 regular map with 10″ spacings of the O_2 774 GHz observations. At this frequency, the beam of the 3.5 m *Herschel* telescope has a size of 28″ (small blue circles). The beam centres for the H- and V-polarisations are separated by 4″.5. Larger (black) circles correspond to the 487 GHz beam positions (44″; cf. Fig. 1) and as before, north is up and east is to the left. Background image is courtesy of *Spitzer* IRAC-MIPS (blue: 3.6 μm, green: 8 μm, red: 24 μm).

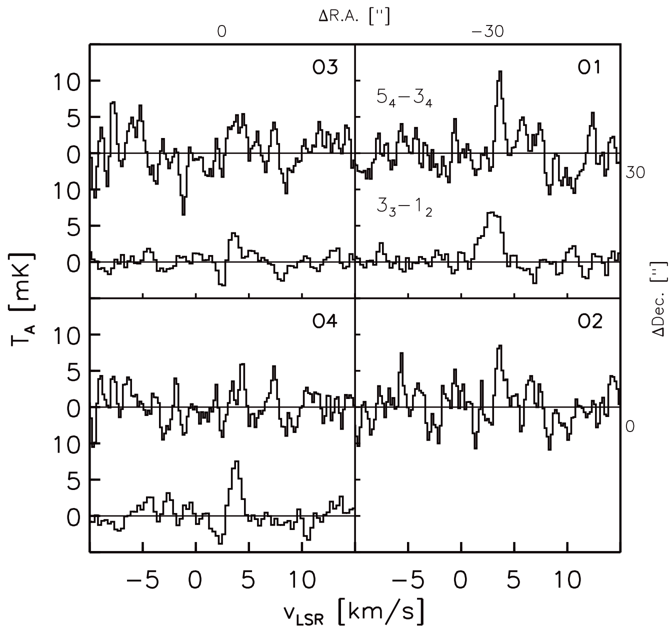

Fig. 4. The WBS spectra toward the positions O1 to O4 are shown for both the 774 GHz (*upper*) and 487 GHz (*lower*) lines in each frame. The average 774 GHz data are convolved to the 487 GHz beam of 44″. Offsets relative to the origin O4 are shown along *the upper and right-hand* scales.

(Liseau et al. 2010), N_2H^+ (1−0) (di Francesco et al. 2004), deuterated molecules (Bergman et al. 2011a) and the recently discovered H_2O_2 (HOOH, Bergman et al. 2011b). For the 2.8 km s^{-1} feature, we are unable to entirely exclude the possibility that it is due to an unidentified species. If so, the line transition frequency should be ν_0 = (487250.548 ± 0.098) MHz (1σ).

3.2. 774 GHz

In Fig. 4 the convolved and averaged 774 GHz spectra are compared to the 487 GHz spectra, and the 6 × 6 map of the 774 GHz observations, convolved to the beam at 487 GHz, is displayed in Fig. 5. The line was not detected toward the east side of the cloud, i.e. toward O3 and O4, with 1σ-upper limits of 3 mK km s^{-1}, but clearly detected toward the west side of the cloud, i.e. toward O1 and O2, at a signal-to-noise ratio of S/N = 4−6. The derived line parameters for the 774 GHz spectra, convolved to the 487 GHz beam, are reported in Table 3. We note that only the 3.6 km s^{-1} component is seen at the O1 position.

The O_2 774 GHz line falls in the lower side band (LSB: 770.75−775.65 GHz). The entire observed spectral region is however totally dominated by the ^{13}CO (7−6) transition at 771.2 GHz. This line exhibits significant variations on small angular scales, which is clearly evident in individual pointings of the 774 GHz beam of width 28″ (FWHM). In the spectrum farthest to the northeast, the line reaches a peak T_{mb} of 25 K, whereas in the opposite corner in the southwest the intensity has decreased to less than 5 K.

In addition, in the upper side band (USB: 783.15−786.815 GHz), the strongest and clearly detected line is due to the C^{17}O (7−6) transition at 786.3 GHz (Larsson et al., in prep.). In contrast to ^{13}CO, the line of C^{17}O reaches its maximum of almost 3 K at the O1 position.

4. Discussion

4.1. Observed quantities: temperature, line width, column density, and size of the O_2 emission region

The O_2 487 GHz and 774 GHz lines are clearly detected toward multiple positions. From the observation of more than one transition, some basic physical parameters of the source can be derived, where we assume that all transitions trace the same gas along the line of sight. In the case of the observed O_2 emission, this should be straightforward, as detailed computations of statistical equilibrium and radiative transfer for a multi-level system demonstrate that this emission is optically thin and originates in conditions of local thermodynamic equilibrium (LTE).

4.1.1. Temperature

At O1, the observed source extent of the 487 GHz and 774 GHz lines appears to be similar, hence the ratio of the beam fillings f_{487}/f_{774} is probably not far from unity. In addition, the main beam efficiencies at these frequencies are also about equal (Table 1). Therefore, the observed ratio of integrated intensities $I(487)/I(774)_{\rm obs}$ is directly comparable to the theoretical one, $I(487)/I(774)_{\rm theo}$, obtained from LTE calculations for optically thin O_2 radiation, which depends only on the gas temperature (Fig. 7).

From Table 4, we see that the measured intensity ratio of the 487 GHz to 774 GHz lines toward O1 implies a temperature of nearly 80 K, with the large error allowing a large range, from about 50 K to very much higher than 100 K (see also Fig. 7). If the beam filling at 774 GHz were smaller than that at 487 GHz, the actual temperatures would be even higher. Our value can

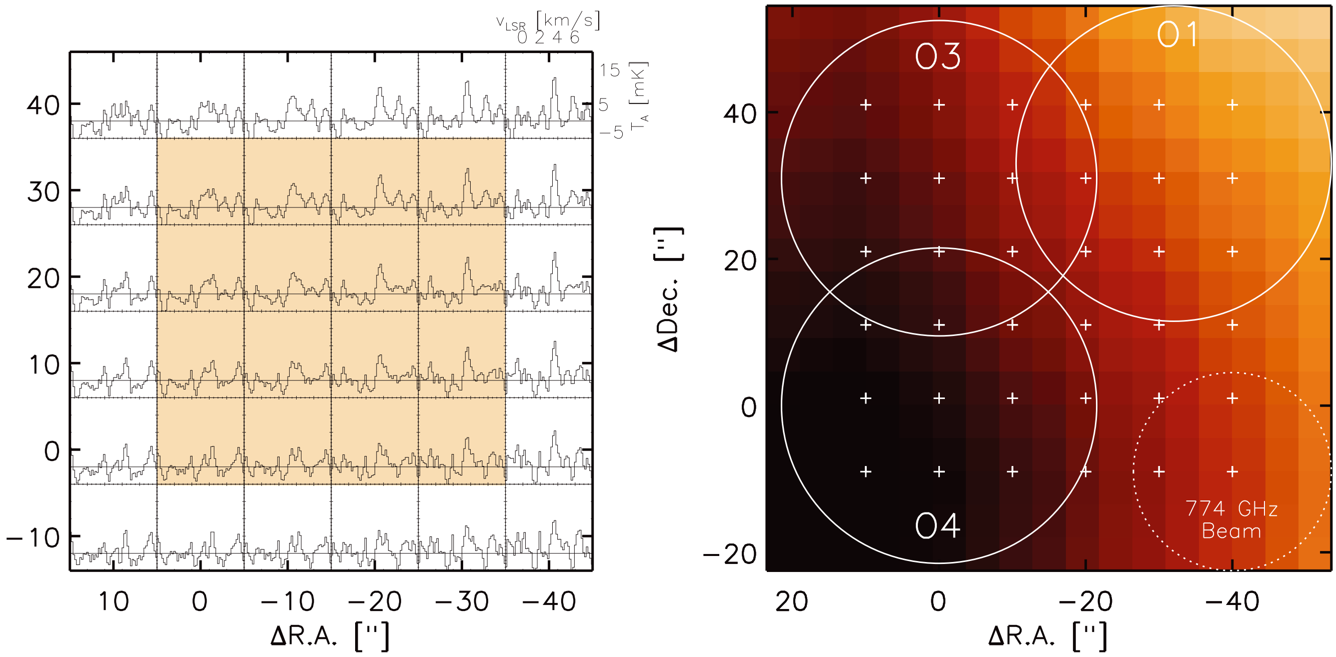

Fig. 5. *Left*: the regridded 6 × 6 map of the WBS 774 GHz spectra, weighted by the Gaussian profile of the 487 GHz beam of 44″. The darker area shows roughly the region within the half power beam width (HPBW). The $\upsilon_{\rm LSR}$ and $T_{\rm A}$ scales are indicated in *the upper right corner*. *Right*: same as *left panel* but as an image of the spatial distribution of the integrated intensity, $\int T_{\rm A}\,{\rm d}\upsilon$, with observed positions shown as pluses. The circles show the 487 GHz and 774 GHz beams, respectively.

Table 4. Observed O_2 line intensity ratios.

Spectrum/ Position	$I(487)^{a,b}$ / $I(774)$	$T_{\rm kin}$ (K)	$N(O_2)$ ($\rm cm^{-2}$)
O1_1 (2.8 km s^{-1})	>0.9 (3σ)	<40	$>2\times10^{15}$
O1_2 (3.6 km s^{-1})	0.58(±0.19)	78	5.4×10^{15}
	(+1σ) 0.77	47	5.0×10^{15}
	(−1σ) 0.39	≫100	…
O3	>0.61 (3σ)	<70	$>3\times10^{15}$
O4	>1.14 (3σ)	<31	$>6\times10^{15}$
⟨O1, O3, O4⟩	1.43(±0.94)^{c}	25	3.4×10^{15}
	(+1σ) 2.37	18	4.6×10^{15}
	(−1σ) 0.49	>100	…

Notes. [(a)] Errors are $\pm(I_1/I_2)\sqrt{(\delta I_1/I_1)^2+(\delta I_2/I_2)^2}$. [(b)] For HIFI, $\eta_{\rm mb}(487)=\eta_{\rm mb}(737)=0.75$. [(c)] Similar to O3 for 1σ limit on 774 GHz intensity (1.47 ± 1.26).

be compared to earlier estimates, obtained at comparable spatial resolution, of both the dust and the gas temperature toward O1. From FIR continuum measurements with a 40″ beam, Harvey et al. (1979) obtained the dust temperature $T_{\rm d}$ = 41 K. Zeng et al. (1984) derived from NH_3 observations, also with a 40″ beam, the temperature of the gas, $T_{\rm g}\sim$ 45 K.

For the dense spot O4 (P 3, SM 1), the 3σ upper limit to the 774 GHz line yields a temperature that is strictly lower than 31 K, which would agree with the value of $T_{\rm g}$ = 22 ± 3 K obtained by Bergman et al. (2011b). For the dense core ρ Oph A, the average for ⟨O1, O3, O4⟩ results in a value of about from 20 K to 25 K, which is entirely consistent with earlier determinations, based on a variety of techniques. Temperaturesbetween 9 K and 49 K have been derived, but with most values clustering around 20−30 K (e.g., Harvey et al. 1979; Loren et al. 1980; Ward-Thompson et al. 1989; Motte et al. 1998; Stamatellos et al. 2007; Bergman et al. 2011a; Ade et al. 2011).

As is also evident from Fig. 5, a temperature gradient or two distinctly different temperature regimes, i.e. higher than about 50 K and strictly lower than 30 K, exist within the boundaries of our limited map of roughly one square arcminute (see also Figs. 1 and 3).

4.1.2. Line width

Comparing the observed line widths, FWHM, of Table 3 with the resolutions offered by the HRS and WBS, we see that the HRS data for the 487 GHz line are all well-resolved ($\delta\upsilon$ = 0.15 km s^{-1}), whereas the 774 GHz line toward O1 and O2 is just barely resolved with the WBS ($\delta\upsilon$ = 0.43 km s^{-1}). However, the average 774 GHz spectrum ⟨O1, O2⟩ is well-resolved with the HRS and the line has a comparable width to that observed with the WBS. It is remarkable that the lines in the cold regions O3 and O4 are observed to be broader than those in the warmer O1 and O2.

The non-thermal contribution to the observed width, $\Delta\upsilon$ = *FWHM*, of an unblended line is $\Delta\upsilon_{\rm nth}=(\Delta\upsilon^2-\Delta\upsilon_{\rm th}^2)^{1/2}$, where all radial velocities are expressed in terms of their FWHM. For T in the range 18 K to 30 K, $\Delta\upsilon_{\rm th}$ = 0.27 to 0.35 km s^{-1}, yielding $\Delta\upsilon_{\rm nth}$ = 0.72 to 0.80 km s^{-1} for the cold region including O3 and O4 (Table 4). Hence, we find that there the line broadening is totally dominated by the non-thermal random motions, which are more than twice as high as the thermal ones. On the other hand, in the warm region O1 and O2, the thermal motions dominate over the non-thermal ones (0.57 km s^{-1} versus ≤0.44 km s^{-1} for T = 78 K) or are comparable at the lower limit temperature of 47 K. This could suggest that, if the non-thermal motions are identified with turbulence at O1 and O2, much of this turbulence has been dissipated and converted into heat.

The O2 source is seen in projection close to the outflow from VLA 1623 and judging from its position (Figs. 1 and 3), it is possible that the gas at O2 is enriched by shock-processed material. At the border of the outflow, a broader line might be expected due to enhanced turbulent motions. The 774 GHz line width appears (marginally) broader than that toward O1 (Table 3), but the uncertainties are large and the significance is low.

4.1.3. Source size

Having determined the temperature, we can use the theoretical line ratio for another transition and equate it to the ratio of the respective beam fillings, e.g. $R \equiv (I_{119}/I_{487})_{\rm theo}(T)/(I_{119}/I_{487})_{\rm obs} = f_{487}/f_{119}$. The relevant 119 GHz data were adopted from Larsson et al. (2007); they are compiled in Table 3 and all lines are displayed on the $T_{\rm mb}$ scale in Fig. 6. For a Gaussian beam at 119 GHz, the beam filling factor is given by $f_{119} \approx \theta^2_{119}/(\theta^2_{119} + \theta^2_{\rm Odin})$, where θ_{119} is the size of the source and $\theta_{\rm Odin}$ that of the beam at 119 GHz. Re-arranging, this reads $\theta_{119} \approx \theta_{\rm Odin}/\sqrt{1/f_{119} - 1} = \theta_{\rm Odin}/\sqrt{R/f_{487} - 1}$, where $\theta_{\rm Odin} = 10'$.

The 487 GHz source seems to be extended on the scale of at least the beam width, i.e. $f_{487} \geq 0.5$, and for the average values of $\langle$O1, O3, O4$\rangle$ in Table 4, we find a size of the Odin source of $\gtrsim$4 to 5 arcmin, for gas at from 18 to 25 K, i.e. for $(I_{119}/I_{487})_{\rm theo}(T) = 11$ to 8, respectively. The solution for much warmer gas (127 K for "-1σ" in Table 4) ought to be excluded, as the calculated source size would exceed $9'$, whereas the 774 GHz line that traces high temperature has been detected only over a limited region ($\lesssim 1'$). On the basis of CS (2−1) mapping observations, Liseau et al. (1995) determined the deconvolved angular size of the densest regions of the ρ Oph A core as $FWHM \sim 4'$ ($n_{\rm H} \gtrsim 10^5$ cm^{-3}), which is consistent with the HIFI and Odin observations of O_2 in ρ Oph A taken together. It appears that the entire ρ Oph A core is faintly glowing in the 119 GHz line.

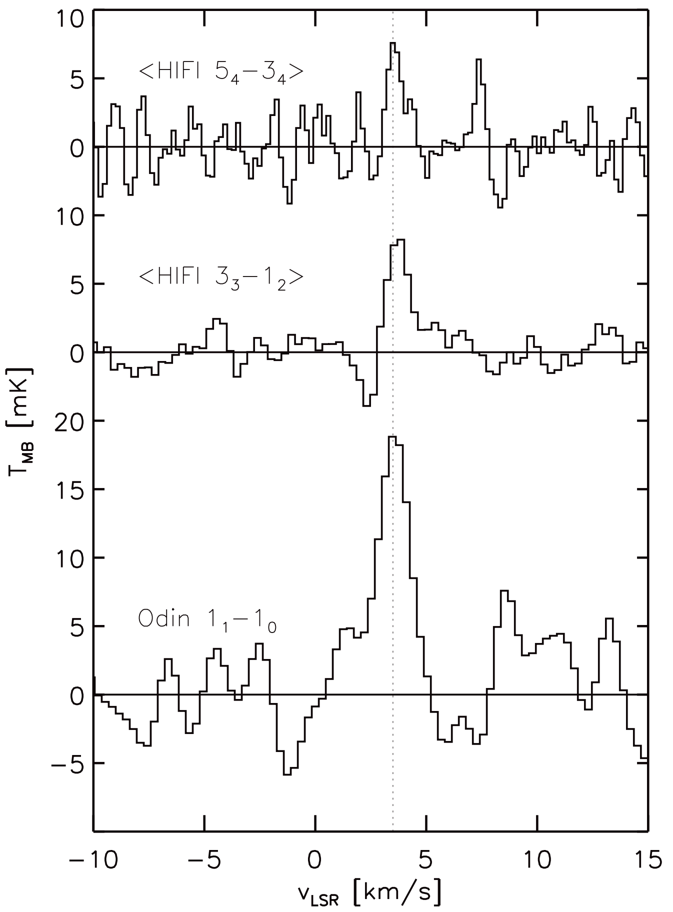

Fig. 6. Average data for the HIFI O_2 observations (774 and 487 GHz) and the Odin 119 GHz spectrum toward ρ Oph A. For proper comparison, these spectra are given on the $T_{\rm mb}$ scale and for reference, a vertical dotted line is shown at $\upsilon_{\rm LSR} = +3.5$ km s^{-1}.

4.1.4. Column density

For the warm region O1, an O_2 column density of 5×10^{15} cm^{-2} is derived, whereas for the cold O4, $N(O_2) > 6 \times 10^{15}$ cm^{-2} (Table 4). These estimations are based on the assumption of optically thin emission in LTE at the kinetic gas temperature $T_{\rm kin}$, i.e. for unit beam filling the O_2 column is given by

$$N(O_2) = \int T_{\rm mb}\,{\rm d}\upsilon \times \Phi(T_{\rm kin})\ \ {\rm cm}^{-2}$$

when the integral is expressed in K cm s^{-1} and where

$$\Phi(T_{\rm kin}) = \left(\frac{2\pi^{1/3}k}{hc}\right)^3 \frac{T^2_{\rm tr}}{g_{\rm ul}A_{\rm ul}} \times \frac{F_\nu(T_{\rm kin})}{F_\nu(T_{\rm kin}) - F_\nu(T_{\rm bg})}\ Q(T_{\rm kin})\ \exp(T_{\rm up}/T_{\rm kin}),$$

in K^{-1} cm^{-3} s (cgs units throughout). Here, the transition temperature is $T_{\rm tr} \equiv h\nu/k$, the quasi-Planck function is $F_\nu(T) \equiv T_{\rm tr}/({\rm e}^{T_{\rm tr}/T} - 1)$, the partition function is $Q(T)$, the upper level energy is $T_{\rm up} = E_{\rm up}/k$ and the other symbols have their usual meaning. The background temperature is that of the cosmic microwave background, i.e. $T_{\rm bg} = T_{\rm CMB}$[1]. The frequencies were adopted from Drouin et al. (2010) and the Einstein A-values from Maréchal et al. (1997) (see also Black & Smith 1984).

On the other hand, if $\langle$O1, O3, O4$\rangle$ were taken as representative of ρ Oph A as a whole, column densities lower than 5×10^{15} cm^{-2} would be derived. Although there is a considerable range in gas kinetic temperature, the O_2 column densities do not seem to vary that much. However, with the observed inhomogeneity of the emission in mind, the significance of such an average could be questioned.

4.2. O_2 abundance

Once the O_2 column density is known, the line-of-sight average O_2 fractional abundance, with respect to H_2 or H-nuclei, can be measured if the column density of H_2 molecules is available. The hydrogen column density along the appropriate lateral and depth scales is not well-known from observations. However, we can get an approximate idea from the $C^{18}O$ observations by Liseau et al. (2010), where it was suggested, based on the line profiles, that the $J = 3{-}2$ line was a reasonably good proxy for the O_2 119 GHz line observed with Odin (Larsson et al. 2007). If the O_2 molecules were indeed cospatial with those of CO and its isotopic variants, their optically thin lines could be used to infer the H_2 column densities relevant also to O_2. We derive "local" $C^{18}O$ column densities by taking $C^{18}O$ intensity and O_2 temperature variations into account. The gas and dust peaks coincide spatially (see also Table 2), i.e. there is no indication of

[1] In our numerical radiative transfer calculations (Sect. 4.1), the dust continuum is also included. These calculations use the collision data of Lique (2010).

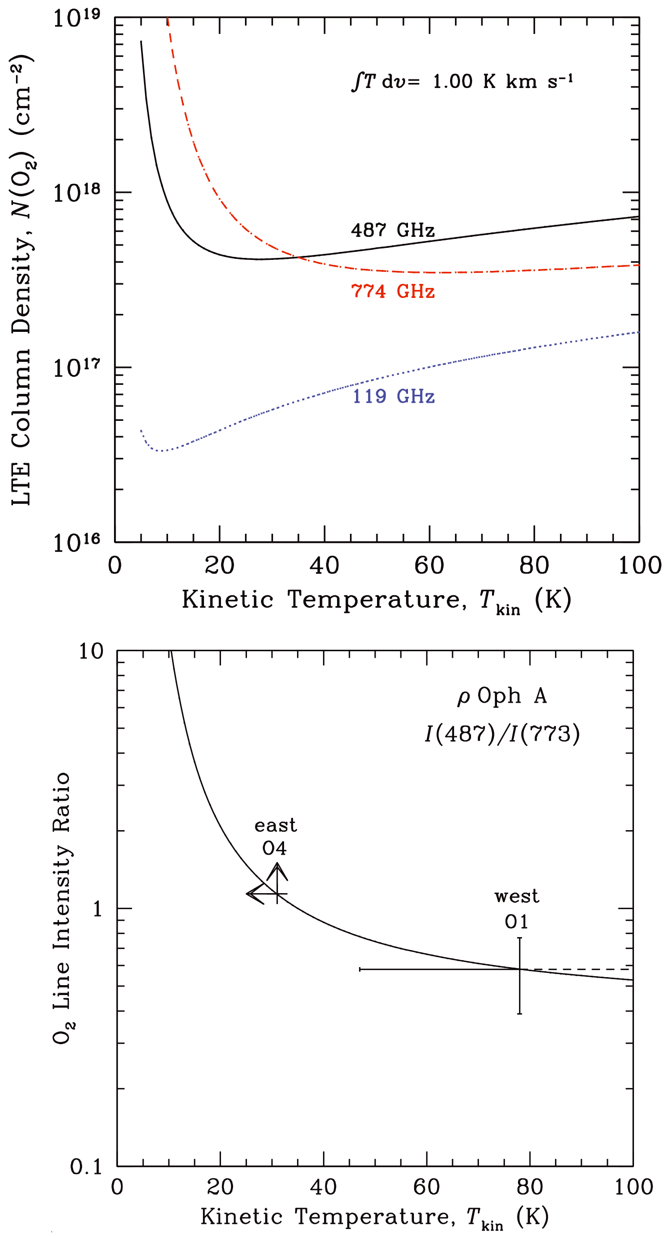

Fig. 7. *Upper*: LTE computations of the O_2 column density $N(O_2)$ as a function of the temperature T for an extended homogeneous source, to yield a line intensity of 1.0 K km s^{-1}. For optically thin emission, intensity and column density are linearly related. 119 GHz: blue dots; 487 Ghz: black solid line; 774 GHz: red short dashes. *Lower*: the ratio of the 487 GHz integrated line intensity to that at 774 GHz is shown by the curve for a range of temperatures. For O1 (=O1_2), the error shown by the dashed line formally extends to the unplausible result of nearly 10^3 K. For O4, the limit symbols are for the lower limit on the intensity ratio and the upper limit on the temperature, respectively.

significant CO freeze out (at levels higher than a factor of 2 to 3, see Fig. 10 of Bergman et al. 2011a). The $C^{18}O$ column density varies by less than 20% for 20 K $\leq T_{\rm kin} \leq$ 50 K. Assuming that $C^{18}O/H_2 = 1.5 \times 10^{-7}$ (likely within about 30%, e.g. Wannier et al. 1976; Goldsmith et al. 2000), H_2 columns are found to be 1×10^{23} cm^{-2}.

Hence, for the O_2 column densities in Table 4, we find that $X(O_2) = 5 \times 10^{-8}$ relative to H_2 in the warm gas toward the west, at O1 (and likely also toward O2), and higher than that toward the east, at the colder O4. The $C^{18}O$ lines are slightly optically thick, implying that these H_2 column densities are lower limits and need to be adjusted upwards by a factor of the order of $\tau/(1-e^{-\tau}) \gtrsim 2$, for $\tau \sim 2$. Hence, these O_2 abundances are upper limits, i.e. the fractional abundance of O_2 in the gas phase is less than indicated above.

A way to obtain a more detailed picture of the source is to use detailed theoretical models to predict the O_2 abundance or column and to compare these models with the observations. This is the topic of the next subsection.

4.3. Chemical models

Specifically for O_2 (and H_2O), Hollenbach et al. (2009) constructed theoretical models of photon-dominated regions (PDRs, Hollenbach & Tielens 1997), invoking also grain surface chemistry, including freeze-out and desorption of the species. These new models are models of the whole cloud, to arbitrary values of the extinction, and show that most of the gas phase O_2, OH, and H_2O is found at values of $A_V \sim 3{-}10$ mag, where the details depend, as in a conventional PDR, on the ratio G_0/n_H. In many aspects, these models are similar to the traditional dense PDR models that include chemistry and gas heating and that explain the abundances and column densities of other molecules (including radicals and ions) at intermediate depths into the clouds (e.g., Fuente et al. 1993; Sternberg & Dalgarno 1995; Jansen et al. 1995; Simon et al. 1997; Pety et al. 2005). The current models are extended even deeper into the cloud where external UV photons no longer play a role in the chemistry, only cosmic-ray induced photons.

In the direction of ρ Oph A, a number of spectroscopic indicators suggest the presence of a PDR[2]. Liseau et al. (1999) inferred that the PDR is situated on the rear side of ρ Oph A, as seen from the Sun, and excited by the two stellar sources HD 147889 and S 1 (see Fig. 1 and Table 2) by their combined UV fields, corresponding to $G_0 \sim 10^2$. For the densest parts of the [C II] emitting ρ Oph A-PDR, these authors empirically derived $n_H = 5 \times 10^4$ cm^{-3} and over more extended regions, from 1 to 3×10^4 cm^{-3}.

The model of Hollenbach et al. (2009) predicts columns of O_2 between about 10^{15} and a few times 10^{16} cm^{-2} depending on the grain temperature in the O_2-emitting region, with higher columns in regions with warmer dust. Warmer (T_d > 20 K) dust produces more O_2 column because O atoms evaporate from grains before they can react with atomic hydrogen sticking to the grains. This increases the elemental gas phase O available to make O_2, whose abundance in the ρ Oph model can locally reach above 10^{-5} for T_d = 25 K. The results are quite insensitive to the gas temperature in the O_2-emitting region for the range 10 K < T_g < 100 K.

However, the Hollenbach et al. (2009) models predict gas temperatures of only ~20 K, as would all thermochemical models with only cosmic ray heating and heating by the penetrating FUV. Gas temperatures as high as 80 K, as derived here, suggest that there are other heating mechanisms, such as slow shocks or turbulent dissipation (e.g., Goldsmith et al. 2010). Our observations show a slight increase in O_2 column in *cooler* gas.

[2] Atomic recombination lines of carbon, ^{12}C, and sulfur, ^{32}S, (Cesarsky et al. 1976; Pankonin & Walmsley 1978), fine structure lines: [C I] 492.2 GHz (Kamegai et al. 2003), [C I] 809.3 GHz (Kamegai et al. 2003; Kulesa et al. 2005), [C II] 157 μm (Yui et al. 1993; Liseau et al. 1999), [O I] 63 μm (Ceccarelli et al. 1997; Liseau et al. 1999), [O I] 145 μm (Liseau et al. 1999; Liseau & Justtanont 2009), and mid-infrared PAH emission (Liseau & Justtanont 2009).

If the dust is also cooler in the cooler gas region, as would be expected for the derived densities above 10^4 and, centrally, higher than 10^7 cm^{-3}, this contradicts the predictions of this particular model.

On the other hand, geometry also plays a role in determining the column of O_2 observed along the line of sight. The Hollenbach et al. (2009) models assume an illuminated slab face-on. However, clumpiness and more edge-on geometry could increase the observed column in some beams, and could explain the slightly higher column of O_2 in the region with somewhat cooler gas. We conclude that these models are modestly consistent with the observations, but likely require some additional gas heating in the O_2-emitting region. We defer detailed thermochemical modelling of these ρ Oph observations to a future paper.

4.4. Source(s) of O_2 or the dearth of O_2

The discussed models could be expected to apply quite generally to all externally illuminated molecular clouds developing PDR-like parts. It is therefore surprising that O_2 has been detected only toward the dense cloud core ρ Oph A (Larsson et al. 2007, and this work) and a spot in OMC-1 (Goldsmith et al. 2011), despite numerous searches toward other regions. For instance, surveying twenty sources, Goldsmith et al. (2000) obtained limiting O_2 abundances $N(O_2)/N(H_2)$ of a few times 10^{-7}, whereas Pagani et al. (2003) derived upper limits to the O_2 column density of 10^{15} to a few times 10^{16} cm^{-2} for nearly a dozen objects. These surveys included dark clouds, regions of low-mass star formation in the solar neighbourhood and of high-mass star formation at different galactocentric distances, i.e. these surveys sampled a wide range of cloud properties and energetics, from quiescent cold clouds to turbulent shock-heated gas caused by mass infall and molecular outflows. Nevertheless, most of these regions escaped detection, although their limiting O_2 column densities fall within the range predicted by the theoretical models.

One possibility could be that this apparent mismatch is due to observational bias, such as source distance and beam dilution. For instance, the limit on the O_2 column in Ori A determined by Pagani et al. (2003) is entirely consistent with the HIFI beam-averaged detection obtained by Goldsmith et al. (2011), if proper correction for dilution in the Odin-beam is applied. We recall that the detected spot is not toward the Orion-PDR (Melnick et al. 2012), as one might have expected, but close to the outflow in the vicinity of IRc 2.

However, the difference in distance aside, ρ Oph A and Ori A represent very different environments in terms of the parameter $G_0/n_{\rm H}$, viz. cold-core deuteration versus hot-core grain chemistry (Bergman et al. 2011a; Bisschop et al. 2007; Ceccarelli et al. 2007; Ratajczak et al. 2011). Star-forming regions such as IRAS 16293 in Ophiuchus, NGC 1333 in Perseus, or the Serpens core near S 68 are more akin to the conditions in ρ Oph A, yet no O_2 detections have been reported. These complexes are at one to two times the distance to ρ Oph A, hence beam dilution issues should be unimportant. It is conceivable that the viewing geometry of ρ Oph A could be particularly favourable for the observability of O_2, although this advantage may not be shared by other regions.

However, a clear difference is suggested by hydrogen peroxide (H_2O_2) only so far having been detected in ρ Oph A (Bergman et al. 2011b). H_2O_2 is thought to be a clear indicator of grain surface chemistry and relatively abundant at about 30 K (e.g., Cazaux et al. 2010).

In the specific model for ρ Oph conditions, Du et al. (2012) find that H_2O_2 is reasonably abundant only for some 10^5 yr (their Fig. 1). A similar, only slightly broader, profile is displayed by the abundance of O_2, rendering this molecule essentially undetectable after about 2×10^5 yr. Compared to other molecular species, which have attained chemical equilibrium and/or are abound on much longer timescales ($>10^6$ yr), the abundances of both H_2O_2 and O_2 appear transient. Therefore, one may expect that the simultaneously detectable abundance of O_2 and H_2O_2 could be used to infer the evolutionary chemical state of the cloud. If that is the case, this may also explain the paucity of known O_2 line emitters.

5. Conclusions

We now summarise the main results of our present study:

- We have successfully detected the 3_3-1_2 transition of O_2 at 487 GHz with HIFI onboard *Herschel* toward three positions in the ρ Oph A core. In addition, we have also obtained a 6×6 oversampled map with $10''$ spacings in the 5_4-3_4 transition at 774 GHz.
- The telescope pointings targeted two cold, high density cores, i.e. O4 [$C^{18}O$ P3 = SM 1] and O3 [$C^{18}O$ P2, near SM 1N], and two positions $30''$ west of these, labelled O2 and O1, respectively. All three observed positions (O1, O3 and O4) were detected in the 487 GHz line, with significant variations in the line intensity on scales as small as $30''$. At 774 GHz, emission was detected from only the western part of the map, including O1 and O2.
- Combining the 487 GHz and 774 GHz data leads to the column density of $N(O_2) > 6 \times 10^{15}$ cm^{-2}, at the 3σ level and at $T < 30$ K, in the high density region O3 and O4, whereas in the warmer region of O1 and O2, $N(O_2) = 5.5 \times 10^{15}$ cm^{-2} ($T > 50$ K). There, our standard analysis yields an abundance of $N(O_2)/N(H_2) \sim 5 \times 10^{-8}$ in the warm gas and somewhat higher in the cold region.
- This result agrees with that for $X(O_2)$ based on the observation of the 119 GHz line with Odin (Larsson et al. 2007), assuming that the O_2 source size has an angular extent of about $5'$.
- The question of why O_2 is such an elusive molecule in the ISM is still unanswered. In the special case of ρ Oph A, there is some evidence that detectable amounts of gas phase O_2 might be a relatively transient phenomenon, which could explain why interstellar O_2 is generally not detected.

Acknowledgements. We appreciate the thoughtful comments by the referee, Prof. Karl Menten, which have lead to an improvement of the manuscript. The Swedish authors are indebted to the Swedish National Space Board (SNSB) for its continued support. This work was also carried out in part at the Jet Propulsion Laboratory, California Institute of Technology, under contract with the National Aeronautics and Space Administration (NASA). We also wish to thank the HIFI-ICC for its excellent support. HIFI has been designed and built by a consortium of institutes and university departments from across Europe, Canada and the US under the leadership of SRON Netherlands Institute for Space Research, Groningen, The Netherlands with major contributions from Germany, France and the US. Consortium members are: Canada: CSA, U. Waterloo; France: CESR, LAB, LERMA, IRAM; Germany: KOSMA, MPIfR, MPS; Ireland, NUI Maynooth; Italy: ASI, IFSI-INAF, Arcetri-INAF; Netherlands: SRON, TUD; Poland: CAMK, CBK; Spain: Observatorio Astronomico Nacional (IGN), Centro de Astrobiologia (CSIC-INTA); Sweden: Chalmers University of Technology MC2, RSS & GARD, Onsala Space Observatory, Swedish National Space Board, Stockholm University Stockholm Observatory; Switzerland: ETH Zürich, FHNW; USA: Caltech, JPL, NHSC.

References

Ade, P. A. R., Aghanim, N., Arnaud, M., et al. 2011, A&A, 536, A20
André, P., Martin-Pintado, J., Despois, D., & Montmerle, T. 1990, A&A, 236, 180
Bergman, P., Parise, B., Liseau, R., & Larsson, B. 2011a, A&A, 527, A39
Bergman, P., Parise, B., Liseau, R., et al. 2011b, A&A, 531, L8
Bisschop, S. E., Jørgensen, J. K., van Dishoeck, E. F., & de Wachter, E. B. M. 2007, A&A, 465, 913
Black, J. H., & Smith, P. L. 1984, ApJ, 277, 562
Caratti o Garatti, A., Giannini, T., Nisini, B., & Lorenzetti, D. 2006, A&A, 449, 1077
Cazaux, S., Cobut, V., Marseille, M., Spaans, M., & Caselli, P. 2010, A&A, 522, A74
Ceccarelli, C., Haas, M. R., Hollenbach, D. J., & Rudolph, A. L. 1997, ApJ, 476, 771
Ceccarelli, C., Caselli, P., Herbst, E., Tielens, A. G. G. M., & Caux, E. 2007, Protostars and Planets V, ed. B. Reipurth, D. Jewitt, & K. Keil (Tucson: University of Arizona Press), 47
Cesarsky, D. A., Encrenaz, P. J., Falgarone, E. G., et al. 1976, A&A, 48, 167
De Graauw, Th., Helmich, F. P., Phillips, T. G., et al. 2010, A&A, 518, L6
Dent, W. R. F., Matthews, H. E., & Walther, D. M. 1995, MNRAS, 277, 193
Di Francesco, J., André, P., & Myers, P. C. 2004, ApJ, 617, 425
Du, F., Parise, B., & Bergman, P. 2012, A&A, 538, A91
Drouin, B. J., Yu, S., Miller, C. E., et al. 2010, JQSRT, 111, 1167
Elias, J. H. 1978, ApJ, 224, 453
Frisk, U., Hagström, M., Ala-Laurinaho, J., et al. 2003, A&A, 402, L27
Fuente, A., Martin-Pintado, J., Cernicharo, J., & Bachiller, R. 1993, A&A, 276, 473
Goldsmith, P. F., & Langer, W. D. 1978, ApJ, 222, 881
Goldsmith, P. F., Melnick, G. J., Bergin, E. A., et al. 2000, ApJ, 539, L123
Goldsmith, P. F., Li, D., Bergin, E. A., et al. 2002, ApJ, 576, 814
Goldsmith, P. F., Velusamy, T., Li, D., & Langer, W. D. 2010, ApJ, 715, 1370
Goldsmith, P. F., Liseau, R., Bell, T. A., et al. 2011, ApJ, 737, 96
Grasdalen, G. L., Strom, K. M., & Strom, S. E. 1973, ApJ, 184, L53
Harvey, P. M., Campbell, M. F., & Hoffmann, W. F. 1979, ApJ, 228, 445
Hincelin, U., Wakelam, V., Hersant, F., et al. 2011, A&A, 530, A61
Hjalmarson, Å., Frisk, U., Olberg, M., et al. 2003, A&A, 402, L39
Hollenbach, D. J., & Tielens, A. G. G. M. 1997, ARA&A, 35, 179
Hollenbach, D., Kaufman, M. J., Bergin, E. A., & Melnick, G. J. 2009, ApJ, 690, 1497
Jansen, D. J., van Dishoeck, E. F., Black, J. H., Spaans, M., & Sosin, C. 1995, A&A, 302, 223
Johnstone, D., Wilson, C. D., Moriarty-Schieven, G., et al. 2000, ApJ, 545, 327
Kamegai, K., Ikeda, M., Maezawa, H., et al. 2003, ApJ, 589, 378
Kulesa, C. A., Hungerford, A. L., Walker, C. K., et al. 2005, ApJ, 625, 194
Larsson, B., Liseau, R., Pagani, L., et al. 2007, A&A, 466, 999
Liseau, R., & Justtanont, K. 2009, A&A, 499, 799
Liseau, R., Lorenzetti, D., Molinari, S., et al. 1995, A&A, 300, 493
Liseau, R., White, G. J., Larsson, B., et al. 1999, A&A, 344, 342
Liseau, R., Larsson, B., Bergman, P., et al. 2010, A&A, 510, A98
Lique, F. 2010, J. Chem. Phys., 132, 04431
Loinard, L., Torres, R. M., Mioduszewski, A. J., & Rodríguez, L. F. 2008, ApJ, 675, L29
Lombardi, M., Lada, C. J., & Alves, J. 2008, A&A, 480, 785
Loren, R. B., Wootten, A., & Wilking, B. A. 1990, ApJ, 365, 269
Mamajek, E. E. 2008, Astron. Nachr., 329, 10
Maréchal, P., Viala, Y. P., & Benayoun, J. J. 1997, A&A, 324, 221
Melnick, G. J., Stauffer, J. R., Ashby, M. L. N., et al. 2000, ApJ, 539, L77
Melnick, G. J., Tolls, V., Goldsmith, P. F., et al. 2012, ApJ, in press
Motte, F., André, P., & Neri, R. 1998, A&A, 336, 150
Nord, H. L., von Schéele, F., Frisk, U., et al. 2003, A&A, 402, L21
Pagani, L., Olofsson, A. O. H., Bergman, P., et al. 2003, A&A, 402, L77
Pankonin, V., & Walmsley, C. M. 1978, A&A, 64, 333
Pety, J., Teyssier, D., Fossé, D., et al. 2005, A&A, 435, 885
Pilbratt, G. L., Riedinger, J. R., Passvogel, T., et al. 2010, A&A, 518, L1
Ratajczak, A., Taquet, V., Kahane, C., et al. 2011, A&A, 528, L13
Roelfsema, P. R., Helmich, F. P., Teyssier, D., et al. 2012, A&A, 537, A17
Simon, R., Stutzki, J., Sternberg, A., & Winnewisser, G. 1997, A&A, 327, L9
Snow, T. P., Destree, J., & Welty, D. E. 2008, ApJ, 679, 512
Stamatellos, D., Whitworth, A. P., & Ward-Thompson, D. 2007, MNRAS, 379, 1390
Sternberg, A., & Dalgarno, A. 1995, ApJ, 99, 565
Wannier, P. G., Penzias, A. A., Linke, R. A., & Wilson, R. W. 1976, ApJ, 204, 26
Ward-Thompson, D., Robson, E. I., Whittet, D. C. B., et al. 1989, MNRAS, 241, 119
Yui, Y. Y., Nakagawa, T., Doi, Y., et al. 1993, ApJ, 419, L37
Zeng, Q., Batrla, W., & Wilson, T. L. 1984, A&A, 141, 127

[1] Department of Earth and Space Sciences, Chalmers University of Technology, Onsala Space Observatory, 439 92 Onsala, Sweden
e-mail: rene.liseau@chalmers.se
[2] Jet Propulsion Laboratory, California Institute of Technology, 4800 Oak Grove Drive, Pasadena CA 91109, USA
[3] Department of Astronomy, Stockholm University, 106 91 Stockholm, Sweden
[4] LERMA & UMR 8112 du CNRS, Observatoire de Paris, 61 Av. de l'Observatoire, 75014 Paris, France
[5] Onsala Space Observatory, Chalmers University of Technology, 439 92 Onsala, Sweden
[6] Observatoire de Paris, LUTH, Paris, France
[7] Centro de Astrobiología, CSICINTA, 28850 Madrid, Spain
[8] Institute of Astronomy, ETH-Zurich, Zurich, Switzerland
[9] Department of Astronomy, University of Michigan, 500 Church Street, Ann Arbor MI 48109, USA
[10] School of Physics and Astronomy, University of Leeds, Leeds, UK
[11] Université de Toulouse, UPS-OMP, IRAP, Toulouse, France & CNRS, IRAP, 9 Av. Colonel Roche, BP 44346, 31028 Toulouse Cedex 4, France
[12] LRA/LERMA, CNRS, UMR8112, Observatoire de Paris & École Normale Supérieure, 24 rue Lhomond, 75231 Paris Cedex 05, France
[13] SETI Institute, Mountain View CA 94043, USA
[14] Department of Physics and Astronomy, San José State University, San Jose CA 95192, USA
[15] National Astronomical Observatories, Chinese Academy of Sciences, A20 Datun Road, Chaoyang District, 100012 Beijing, PR China
[16] California Institute of Technology, Cahill Center for Astronomy and Astrophysics 301-17, 1200 E. California Boulevard, Pasadena CA 91125, USA
[17] Harvard-Smithsonian Center for Astrophysics, 60 Garden Street, MS 66, Cambridge MA 02138, USA
[18] SRON Netherlands Institute for Space Research, PO Box 800, 9700 AV, and Kapteyn Astronomical Institute, University of Groningen, Groningen, The Netherlands
[19] Department of Astronomy, University of Massachusetts, Amherst MA 01003, USA
[20] Leiden Observatory, Leiden University, PO Box 9513, 2300 RA Leiden, The Netherlands
[21] Max-Planck-Institut für Extraterrestrische Physik, Gießenbachstraße 1, 85748 Garching, Germany
[22] Department of Physics and Astronomy, University College London, London, UK